Chiral Induction with Chiral Conformational Switches in the Limit of Low "Sergeants to Soldiers" Ratio

Ajiguli Nuermaimaiti,[†] Christian Bombis,[†] Martin M. Knudsen,[‡] Jacob R. Cramer,[‡] Erik Lægsgaard,[†] Flemming Besenbacher,[†] Kurt V. Gothelf,[‡] and Trolle R. Linderoth[†,*]

[†]Sino-Danish Center for Molecular Nanostructures on Surfaces, Interdisciplinary Nanoscience Center (iNANO) and Department of Physics and Astronomy, Aarhus University, Gustav Wieds Vej 14, 8000 Aarhus C, Denmark and [‡]Sino-Danish Center for Molecular Nanostructures on Surfaces, Interdisciplinary Nanoscience Center (iNANO) and Department of Chemistry, Aarhus University, Langelandsgade 140, 8000 Aarhus C, Denmark

ABSTRACT Molecular-level insights into chiral adsorption phenomena are highly relevant within the fields of asymmetric heterogeneous catalysis or chiral separation and may contribute to understand the origins of homochirality in nature. Here, we investigate chiral induction by the "sergeants and soldiers" mechanism for an oligo(phenylene ethynylene) based chiral conformational switch by coadsorbing it with an intrinsically chiral seed on Au(111). Through statistical analysis of scanning tunneling microscopy (STM) data, we demonstrate successful chiral induction with a very low concentration of seeding molecules down to 3%. The microscopic mechanism for the observed chiral induction is suggested to involve nucleation of the intrinsically chiral seeds, allowing for effective transfer and amplification of chirality to large numbers of soldier target molecules.

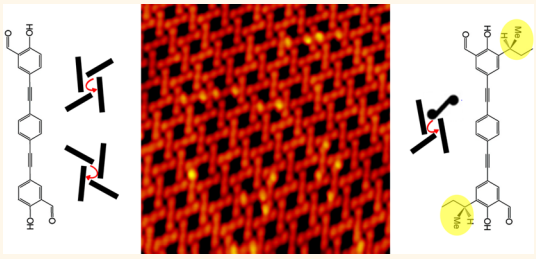

KEYWORDS: Au(111) · molecular self-assembly · chiral induction · homochiral surface · molecular conformations · scanning tunneling microscopy

Adsorption and organization of chiral and prochiral molecules on surfaces has been intensely studied recently, not least by the technique of scanning tunneling microscopy (STM).[1−4] The molecular-level insights into chiral adsorption phenomena achieved by these efforts will benefit, *e.g.*, asymmetric heterogeneous catalysis[5] or chiral separation and sensing[6] and may contribute to understand the origins of biomolecular homochirality.[7]

In chiral induction[8−10] the aim is to steer the chirality of an adsorption system toward a single handedness. Chiral induction has been achieved using external agents such as solvent molecules[11,12] or applied fields[12,13] as well as by energetic/kinetic effects which amplify a small enantiomeric excess in the adsorption system, an approach known as the "majority rule".[14,15] Chiral induction may also be achieved through coadsorption of target molecules with another compound acting as chiral induction agent, often referred to as the "sergeants and soldiers" approach to chiral induction.[16] The classical example of the sergeants and soldiers effect in a surface adsorption system under ultrahigh vacuum conditions is the use of enantiopure tartaric acid as an induction agent (sergeant) for the structurally related, but achiral succinic acid (soldier).[17] Enantiospecific substitution in this model system has later been observed by STM[18] as well as sergeants and soldiers chiral induction in a number of related adsorption systems.[10,19] At liquid−solid interfaces, chiral induction has in particular been achieved in nanoporous molecular assemblies formed from complex target molecules both using chiral induction agents synthesized to closely resemble the target molecules[20] and for structurally simple induction agents.[21,22] Recent studies have started to unravel the microscopic mechanisms underlying chiral induction by the sergeants and soldiers approach. In several systems, the coadsorbed chiral agents induce chiral conflict *i.e*, they preferentially render domains of one handedness disordered while leaving the corresponding mirror domains unaffected.[10,23] There is thus need for further investigations of induction mechanisms where the induction agent acts directly as a chiral

* Address correspondence to trolle@inano.au.dk.

Received for review April 15, 2014 and accepted June 24, 2014.

Published online June 24, 2014
10.1021/nn502097h

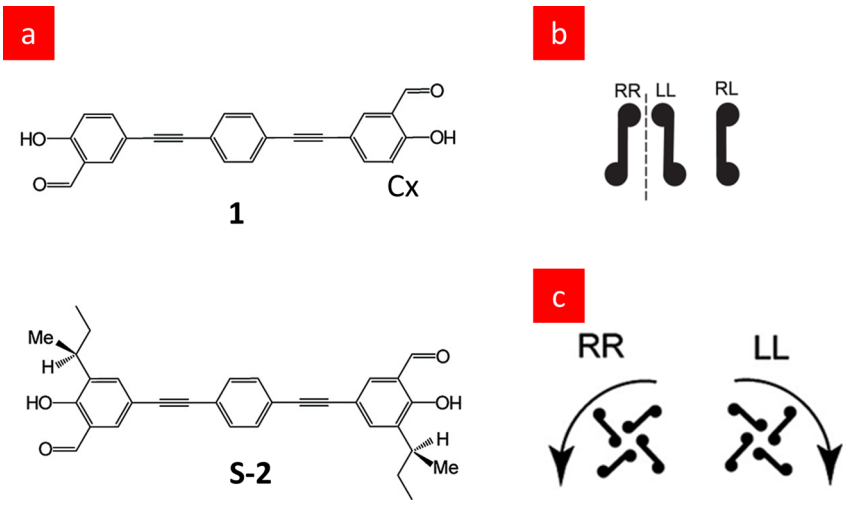

Scheme 1. (a) Molecular model system based on rod-shaped molecules with oligo(phenylene-ethynylene) (OPE) backbones and salicylaldehyde terminal groups. Compared to the prochiral soldier molecule 1, the intrinsically chiral sergeant molecule S-2 in addition contains two chiral (*S*)-*sec*-butyl groups. (b) Schematic representation of conformations assumed after adsorption. Black circles represent the orientation of the (*S*)-*sec*-butyl group in S-2 (or the hydrogen atom saturating the Cx-atom in 1), while black rods represent the OPE molecular backbone. The R and L (right and left) nomenclature refers to the position of the Cx-atom/(*S*)-*sec* butyl group with respect to the molecular backbone when observing it from the central benzene ring. For 1, the RR and LL conformers constitute mirror image surface enantiomers, which occur with equal probability. For S-2, the interaction of the chiral (*S*)-*sec*-butyl groups with the surface leads to a preference for the RR conformation. (c) Schematic representation of windmill motifs formed by molecules in RR and LL conformation, respectively.

seed and steers the chirality of all target molecules toward one handedness. Previously, we reported upon sergeants and soldiers chiral induction in a model system of conformational chiral switches, *i.e.*, molecules which can change between enantiomeric forms on the surface through conformational dynamics. In this system, prochiral rod-shaped molecules self-assemble into organizationally chiral windmill structures.[24] Trough coadsorption with a structurally similar but intrinsically chiral analogue,[25] we achieved selective formation of windmill domains with one handedness.[26] These experiments provided molecular-level observations of two different mechanisms for chiral induction in the form of either kinetically dominated nucleation of the chiral sergeant molecules, or thermodynamically dominated intermixing of sergeants and soldiers. The intermixing protocol was shown to lead to essentially perfect transfer of chirality to the prochiral soldier molecules, but this was achieved, however, at a fairly high ratio of sergeants to soldiers approaching 1:1.

Here, we expand on this previous study of chiral induction for conformational switches. In particular, we explore the lower limit for the fraction of seeding molecules necessary to induce a chiral bias. Through statistical analysis of UHV-STM data, we demonstrate successful chiral induction with a very low fraction of seeding molecules down to 3%. On the basis of the distribution of seeding molecules in the final growth structures, we discuss the microscopic mechanism for chiral induction and suggest it involves nucleation of the intrinsically chiral seeds, allowing for effective transfer and amplification of chirality to large numbers of soldier target molecules.

RESULTS AND DISCUSSION

The molecular model system utilized in this study is illustrated in Scheme 1a. The seeding compound **S-2** consists of an oligo(phenylene-ethynylene) (OPE) backbone which is functionalized with carbonyl and hydroxyl groups as well as two chiral (*S*)-*sec*-butyl groups rendering it intrinsically chiral. In our previous experiments the target molecules subjected to induction closely resembled these seeding molecules, the only difference being that the (*S*)-*sec*-butyl groups on **S-2** were replaced with *tert*-butyl groups, which have the same empirical formula but are achiral. In the present study we use instead the simpler target molecule **1** in which these bulky side groups are replaced by H atoms. The chemical synthesis and the adsorption structures formed by these compounds alone were described previously.[25,27] The motivation for using **1** is partly to explore if the chiral induction also functions for molecules with a larger structural difference, and partly because **1** was previously observed to selectively form wind-mill assemblies on the surface, in contrast to our original target molecule which also forms an organisationally achiral brickwall structure.[27]

When probing the Au(111) surface with STM after codeposition of **1** with a small fraction of **S-2** we observe that the molecular backbones are organized in networks as shown in Figure 1. The network is based on a windmill motif built by four molecules and displays organizational chirality as expressed by the sense of rotation of the windmill motifs which can be arranged in either clockwise or counterclockwise order (Scheme 1c and Figure 1b). From the high-resolution

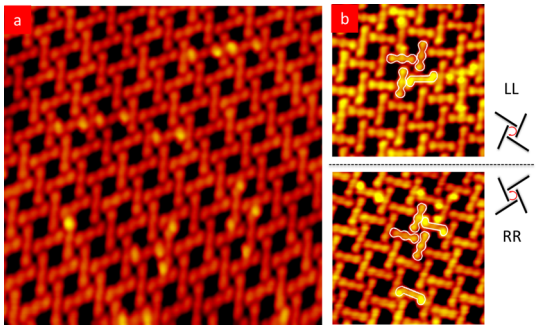

Figure 1. Windmill structures formed on Au(111) by intermixing of 1 with a low concentration of S-2. (a) Large-scale overview image (300 Å × 300 Å). The (*S*)-*sec*-butyl groups of S-2 are imaged as bright protrusions next to the OPE backbone, allowing to distinguish S-2 from 1 and to identify the conformation of the S-2 molecules. (b) High resolution images (100 Å × 100 Å) showing the clockwise (counterclockwise) oriented windmill structures consisting of LL (RR) enantiomers of 1. Different conformers of S-2 are indicated.

images in Figure 1a, we can distinguish **S-2** and **1** in the windmill islands based on the bright protrusions found slightly offset from the central backbone on a few of the molecules. The protrusions can be attributed to the (*S*)-*sec*-butyl groups of **S-2** as established from comparison with STM images of the individual compounds[25,27] (Supporting Information). The imaging of the bulky *sec*-butyl group as a prominent protrusion is also known from previous investigations with this and similar molecules.[24] The different surface conformers of **S-2** can be distinguished from the positions of the bright *sec*-butyl protrusions as illustrated in Scheme 1b. When looking along the central spoke from the center of a molecule, the (*S*)-*sec*-butyl group can be placed either on the left (L) or on the right (R) side of the molecule. The salicylaldehyde groups alone are not sufficiently well resolved in the STM images to distinguish between different conformations of **1.** However, we have shown[27] that the pronounced chiral organization in the windmill motifs is strongly correlated with molecular conformational chirality, most likely owing to the formation of intermolecular hydrogen bonds toward the node center mediated by the aldehyde moieties. Hence, the clockwise oriented windmills exclusively consist of LL molecular conformers and the counterclockwise oriented mirror windmills of RR conformers, which are surface enantiomers (Scheme 1c). This organization implies that the hydrogen atoms saturating the Cx atoms of the outer rings are placed at the outside of the windmill nodes as also found for the (*S*)-*sec*-butyl groups of compound **S-2** forming similar windmill structures when adsorbed alone on Au(111).[25]

Figure 1b highlights a clockwise oriented windmill node consisting of three **1** and one **S-2** molecule in the LL conformation. Similarly, a counterclockwise oriented node from a different domain is shown, containing one RR conformer of the **S-2** molecule. These images show

TABLE 1. Statistical Results for the Concentration of Different Molecular Conformers of S-2 within RR and LL Domains as Well as Globally for All Domains[a]

S-2 molecules	RR domains	LL domains	all domains
RR	10.6 ± 1% (425/4018)	0	7.5 ± 1% (425/5667)
LL	0	7.6 ± 1% (126/1649)	2.2 ± 1% (126/5667)
RL/LR	2.2 ± 0.2% (88/4018)	1.0 ± 0.2% (17/1649)	1.9 ± 0.2% (105/5667)

[a] The data set is based on observation of 5011 **1** and 656 **S-2**.

that the LL or RR conformers of **S-2** organize in the same way as **1** alone when they are embedded in the windmill structure formed from **1**: The molecular head joins a neighboring molecule in nearly orthogonal fashion at a position between the central and outermost benzene ring. The similar packing suggests a similar intermolecular hydrogen bonding motif as proposed for **1** alone.[27] Somewhat surprisingly, we also observe RL/LR conformers of **S-2** within the windmill domains as highlighted in Figure 1b for an RR domain. The stacking of the **S-2** molecules in RL conformation does not differ from the stacking found for **S-2** in the preferred conformation (here RR), presumably because of constraints formed by the surrounding molecules and/or formation of an alternative intermolecular hydrogen bond. Most importantly, these results show that **1** and **S-2** intermix well despite their structural differences. We do not observe segregation in the form of separate islands formed exclusively by one of the compounds. This intermixing is a prerequisite to achieve local transfer of chirality from the seeds to the target molecules.

To quantify the distribution of the compounds we counted the molecular types and conformers and determined the concentration of different molecular conformers of **S-2** embedded in the respective windmill domains formed by **1.** Results from this analysis are reported in Table 1. The fraction of **S-2** is similar within the RR and LL domains with a slight preference for embedding in the RR domains. In both types of windmill domains, we observe the RL/LR molecular conformers of **S-2** at low concentration. Since formation of the optimal intermolecular bonding motif will be prevented at the node centers where the **S-2** molecules assume the unpreferred conformation, we consider the **S-2** molecules in RL conformations as structural defects. Since we never observe RR (LL) molecular conformers of **S-2** in the opposite LL (RR) organizational domains, the energy cost of forming this structural defect must be sufficiently high that it does not occur at both ends of the **S-2** molecules. Overall in this data set, we observe a significantly higher number of RR conformers of **S-2** (7.5%) compared to LL conformers (2.2%) already indicating the anticipated chiral bias of the seeding molecules. The preference for RR conformations of **S-2** is believed to

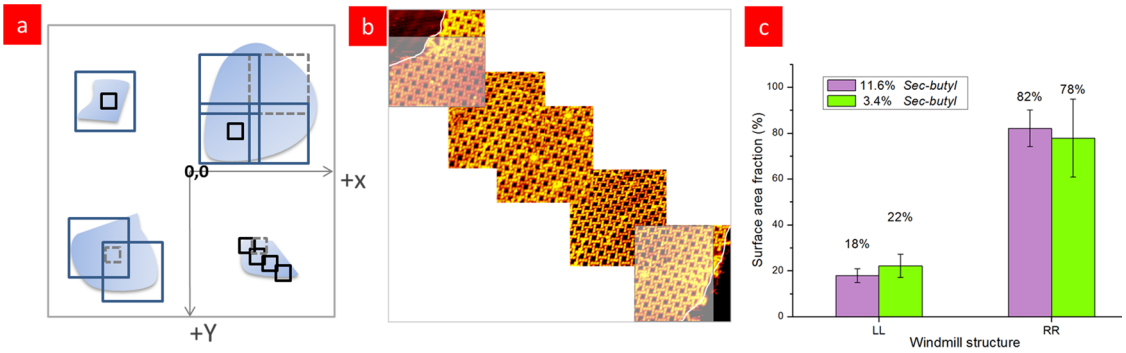

Figure 2. (a) Schematic illustration of how the crystal surface is surveyed at one macroscopic spot. The accessible 2 × 2 μm^2 scanner range is indicated by the large gray square and the position within this area is known from the scanner tube offset voltages. Molecular islands are sketched in blue. The top left island is small enough to be imaged entirely with a medium scale image (blue square), and its chirality is subsequently resolved by a zoomed-in image (small black square). The large island on the top right is surveyed by several medium sized images. As shown for the bottom left island, sudden loss of tip resolution can occur (dashed gray squares) preventing determination of the domain chirality. The bottom right island is assessed by overlapping tiles of images which provide both high resolution (individually) and area determination (in combination). (b) Example of a tiling made from 5 STM images (300 Å × 300 Å) offset according to the position at which they were acquired, thereby providing a larger overview of a windmill domain with sufficient resolution to determine its organizational chirality (here RR). In cases where domain boundaries are imaged, the area is estimated from an approximating rectangle as indicated. This approach was judged not to induce significant uncertainties in the area determination. (c) Histograms showing the overall area fractions of RR and LL windmill domains as determined from this analysis.

result from preferential interaction of the chiral (*S*)-*sec*-butyl groups with the surface when the molecular end-group is in the R conformation compared to L.[25]

To establish whether chiral induction is globally successful, the areas covered by RR and LL windmill domains, respectively, must be determined. This determination is a nontrivial task since STM is a local probe technique. To gain an integrated picture, an extensive survey of different spots on the crystal surface is required as the windmill structures occur as sparse domains separated by free surface. The challenge is compounded by the conflicting demands placed on the scanning conditions to achieve (i) large-scale images to determine island areas and (ii) small-scale images with sufficient molecular resolution to identify the chiral sense of the windmill structures and the conformations of the embedded **S-2** molecules. The strategies we employed to overcome these challenges and systematically survey the surface are illustrated in Figure 2a. Initially, we attempted to record several medium-sized images to assess the surface area covered by an island followed by high-resolution images obtained by zooming in within the island. However, we experienced practical difficulties with this method as the frequent changes in image scale often lead to loss of tip resolution, which rendered the inspection inefficient. We therefore adopted a better strategy where an overlapping cascade of images were acquired, each with the maximum possible size still providing sufficient resolution to determine the domain chirality. An example of a resulting tiling of STM images is shown in Scheme 2b. In the evaluation of windmill domain areas, we summed all observed areas taking due account of overlapping images.

Table 2 (top row) and Figure 2c summarizes results from the analysis of areas. We find twice as many RR domains (34) as LL domains (17), and the observed total area of RR domains (30100 kÅ^2) is much larger than that of LL domains (6500 kÅ^2). Of the observed soldier molecules (**1**), 82 ± 8% are thus organized in RR domains (Figure 2c). As mentioned above, it was usually not possible to image the windmill islands in their entirety. From inspection of our data we find that 40% of the observed LL domains could be imaged entirely, while this was in contrast never possible for the RR domains. This observation strongly suggests that the RR domains are systematically larger in size than the LL domains. The sampling is thus likely to have underestimated the area of RR domains relative to LL domains. From Figure 2c we therefore conclude that chiral induction has been achieved and that it is most likely even more pronounced than indicated by the histogram.

In this first set of experiments, the global fraction of **S-2** was ∼12% (11.6 ± 0.5%) averaging over all domains. To explore the minimum amount of chiral seeds necessary to allow chiral induction, we performed a second set of experiments where we lowered the concentration of **S-2** to ∼3%. The results from these experiments (Table 2 bottom row) are qualitatively the same as observed for ∼12% seeds. The histograms plotted in Figure 2c for different seeding concentrations also agree quantitatively within the uncertainties. Lowering the concentration of seeding molecules, therefore, appears not to appreciably diminish the induction effect. In summary, our observations demonstrate that global chiral induction is achieved for this system of "sergeants" (**S-2**) and "soldiers" (**1**) down to a very low concentration of 3% for the sergeant molecules.

To illuminate the mechanism of chiral induction, we have further analyzed the intermixing of the two

TABLE 2. Statistical results for numbers and areas of LL and RR windmill domains observed after chiral induction. The upper row is for experiments with an overall S-2 (sergeant) fraction of ~12% while the bottom row is for a fraction of ~3%

concentration of S-2 molecules			population of LL/RR doamins		observed area of LL/RR domains (10^6 Å^2)	
all domains	LL domains	RR domains	LL domains	RR domains	LL	RR
11.6 ± 0.5% (656/5667)	8.7 ± 1% (143/1649)	12.8 ± 1% (513/4018)	33 ± 9% (17/51)	67 ± 15% (34/51)	6.5	30.1
3.4 ± 0.5% (78/2266)	3.3 ± 0.5% (24/721)	3.5 ± 1.5% (54/1545)	39 ± 12% (14/36)	61 ± 17% (22/36)	5.7	14.8

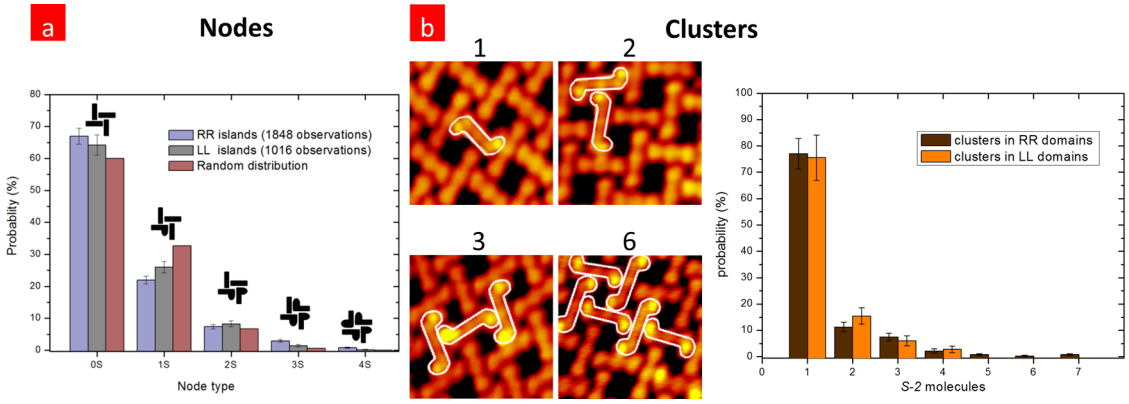

Figure 3. (a) Analysis of node types observed in windmill domains divided according to the number of participating S-2 molecules. The random distribution is a binomial distribution calculated for the probabilities $P_{S\text{-}2}$ = 0.12 and P_1 = 0.88. (b) Cut-outs from STM images showing clusters containing 1, 2, 3, and 6 S-2 molecules (highlighted by outlines) embedded in windmill domains of 1. Histogram on the right: Normalized cluster size distribution as obtained from analysis of 397 clusters in RR domains and 181 clusters in LL domains.

compounds for the set of experiments with ~12% **S-2**. The intermixing is quantified by analyzing the nodes where four molecules join in the windmill structures. Figure 3a shows the probabilities of finding nodes involving 0, 1, 2, 3, or 4 **S-2** molecules, respectively (0S to 4S nodes). Since the fraction of **S-2** is low, the vast majority of the nodes (~75%) are 0S, *i.e.*, formed exclusively by **1**. As expected, the probability distribution decays rapidly for an increasing number of **S-2** molecules participating in the nodes, but even observations of 4S nodes do occur. This qualitative behavior is observed independently of the organizational chirality (LL/RR) of the windmill domains. To compare with the situation for a random distribution, we have calculated a binomial distribution assuming the probabilities of **S-2** and **1** in the nodes to be equal to the fraction of these molecules in the structure. The experimentally observed probabilities deviate in a significant way from those for the random situation: Nodes containing more than one (*S*)-*sec*-butyl group are slightly more often observed in the experiment compared to the random distribution while there are significantly fewer nodes containing only one (*S*)-*sec*-butyl group. (Note that since the two ends of the **S-2** molecules are connected, the end-groups are not completely independent as assumed in the calculated distribution. To see the consequence of this effect, consider the extreme case of one **S-2** molecule in a windmill matrix. Here it is only possible to form two 1S nodes but not a 2S node. A random distribution including this effect would thus contain more 1S and less 2S nodes than the calculated distribution show, causing it to deviate even further from the experimental situation.) From Figure 3a we therefore conclude that while **1** and **S-2** intermix well and do not phase separate, there is nevertheless a tendency toward clustering of the **S-2** seeds within the windmill domains.

Figure 3b shows examples of clusters of **S-2** embedded in windmill domains of **1**. The cluster size is defined as the number of **S-2** molecules linked to each other, either directly or via other **S-2** molecules. The observed size distribution for such clusters is plotted in Figure 3c. A majority of clusters are single molecules (75−80%), and the probability decays rapidly with cluster size, but clusters of sizes up to 7 **S-2** molecules are observed. The tendency toward clustering appears independent of the domain chirality.

The observed clustering suggests a nucleation mechanism for the observed chiral induction. We hypothesize the following microscopic scenario (Scheme 2): After codeposition of seeding and target molecules, we slightly annealed the sample to T_1 = 320 K. Since we have never observed stable molecular islands from

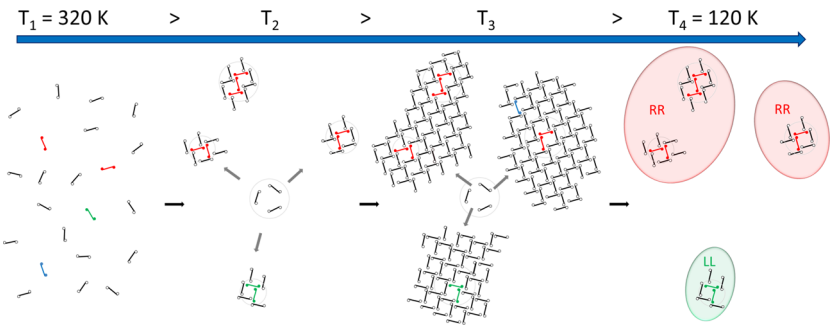

Scheme 2. Schematic illustration of the chiral induction mechanism. At T_1, S-2 and 1 intermix as a 2D molecular gas. Different conformations of the molecules are shown as introduced in Scheme 1b. S-2 molecules are colored according to conformation: red (RR), green (LL), or blue (RL/LR), while target molecules are shown in black. At T_2, nuclei of S-2 molecules start to form showing a preference for RR conformation. At T_3, growth occurs by accommodation of the chiral switches 1. Coalescence is more likely to occur for the majority RR islands. At T_4, domain growth and coalescence is finished resulting in more and larger RR domains compared to LL domains.

this family of molecules at such high temperature, we expect that the compounds perfectly intermix in a 2D molecular gas. Starting from T_1 = 320 K, we slowly cooled the sample to the imaging temperature of $T_4 \approx$ 120 K. On the basis of the observed clustering behavior (Figure 3), we suggest that during this cool-down, nucleation of **S-2** clusters occurred slightly before nucleation/immobilization of the target molecules **1**. This suggestion is supported by the observation that windmill islands of the target molecule **1** were found to start dissolving already at 160−180 K (Figure S3), whereas islands of **S-2** molecules have previously been observed to be stable at 200 K,[26] indicating that the homomolecular interaction of **S-2** is slightly stronger than that for **1**. The seeding molecules **S-2** have a preference for the RR conformational state owing to different interaction of the (*S*)-*sec*-butyl group with the surface in R and L conformation.[25] More RR than LL nuclei will thus form. Since the soldier molecules **1** are chiral conformational switches which can change chirality by thermally induced rotations of the outer rings around the molecular length axis,[24,27,28] all target molecules arriving at an island boundary can be incorporated irrespective of their conformational chirality. Chiral accommodation[24] thus enables the preferred formation of RR islands to be maintained during the growth process. The observation of larger RR domains may be a result of domain coalescence which is more likely to occur for the majority domain type.

It is interesting to compare this scenario to the situation in our previous experiments[25] where chiral induction was performed with the same sergeant molecule (**S-2**) but a different soldier molecule with closer similarity to **S-2** (the *sec*-butyl groups in **S-2** were replaced by achiral *tert*-butyl groups). For this previously investigated soldier molecule, thermally stable islands have been observed up to 220 K[24] suggesting that its homomolecular interactions are similar to those for **S-2** and stronger than for the current soldiers (**1**). In this case, chiral induction was achieved by either (i) a kinetically dominated nucleation approach or (ii) a thermodynamically dominated intermixing approach. In the nucleation approach stable windmill islands of **S-2** (with a strong RR bias) where formed first and subsequently the soldier molecules were added at a temperature low enough to ensure that the preformed windmill islands were not destroyed. In the intermixing approach, the sergeants and soldiers were codeposited and subsequently annealed to allow them to intermix. The intermixing approach was most effective with respect to chiral induction since chirally unbiased nucleation and growth of soldier islands was avoided. However, the intermixing was performed with a relatively high fraction of sergeant molecules (42%) ensuring that most soldier molecules were in direct contact to sergeant molecules. In this earlier investigation, the limit of a low fraction of sergeant molecules was not probed. But we believe the presently investigated sergeant-soldier system is more effective with respect to chiral induction by seeding owing to the larger difference in homomolecular interaction strengths between sergeants and soldiers. This difference allows nucleation of sergeants to start before chirally unbiased nucleation of soldiers occurs to any appreciable degree.

The observation of chiral induction with down to 3% sergeant molecules is comparable to the classic tartaric acid-succinic acid system where only 2% enantiopure tartaric acid (sergeant) was observed to induce chirality in the assembly of achiral succinic acid (soldier)[17] (albeit without microscopic observation of the induction mechanism). Another example of chiral induction with a very low fraction of sergeant molecules was recently described for cyclic porous molecular networks.[20] Here, the induction was attributed to a hierarchical chiral recognition mechanism and a thermodynamic preference for the energetically favored domain chirality. The observation in the present study that the chiral induction effect is similar for 12% and 3% sergeant molecules suggests that 3% is not the minimum amount necessary to achieve a pronounced

induction effect. Indeed, the proposed nucleation mechanism for the chiral induction makes it plausible that chiral induction could be achieved for even lower concentrations of sergeant molecules.

CONCLUSION

In summary, we have investigated the "sergeant and soldiers" principle for chiral induction with molecular switches. By means of a thorough UHV-STM investigation, we have demonstrated successful chiral seeding at very low concentrations of seeding molecules down to 3%. Our microscopic observations suggest that a nucleation mechanism is responsible for the successful chiral seeding and demonstrate that chiral induction using conformational switches is an effective approach for creating chiral surfaces.

METHODS

The experiments were performed in a UHV system with a base pressure in the low 10^{-10} mbar regime and equipped with a home-built variable temperature Aarhus STM. The Au(111) single crystal was cleaned by several cycles of 1.5 keV Ar^+ sputtering followed by annealing at 850 K, resulting in an atomically clean ($22 \times \sqrt{3}$) herringbone reconstructed Au(111) surface. The synthesis of the molecules has been described previously for **1**[27] and **S-2**.[25] The intrinsically chiral molecule **S-2**, which is substituted with an (*S*)-*sec*--butyl group, was obtained by an elaborate enantiospecific synthesis, and the corresponding enantiomer was not available for study. The molecules were sublimated from separate, resistively heated glass crucibles maintained at 375 K (**S-2**) and 360 K (**1**) and held within a few centimeters from the Au surface. Typical dosing times were 4 min resulting in submonolayer coverage. STM images were acquired in the temperature range of 100−140 K. We followed the previously described[26] "intermixing protocol" and dosed both compounds sequentially onto a Au(111) surface held at room temperature (300 K). Subsequently, the sample was annealed at 320 K for 30 min after which it was slowly cooled over a period of 1 h to 120 K. STM images were recorded in the constant current mode with tunneling parameters of I_t = 0.2−0.4 nA and U_t = −1.0 to −1.8 V.

Conflict of Interest: The authors declare no competing financial interest.

Supporting Information Available: Additional adsorption structures observed for **1** and **S-2**. Information on the themal stability of the windmill structure formed by **1**. This material is available free of charge via the Internet at http://pubs.acs.org.

Acknowledgment. We acknowledge financial support from the Marie-Curie ITN SMALL, The Danish Council for Independent Research - Natural Sciences, The Villum Foundation and the Danish National Research Foundation.

REFERENCES AND NOTES

1. Raval, R. Chiral Expression from Molecular Assemblies at Metal Surfaces: Insights from Surface Science Techniques. *Chem. Soc. Rev.* **2009**, *38*, 707–721.
2. Elemans, J. A. A. W.; De Cat, I.; Xu, H.; De Feyter, S. Two-Dimensional Chirality at Liquid-Solid Interfaces. *Chem. Soc. Rev.* **2009**, *38*, 722–736.
3. Ernst, K. H. Supramolecular Surface Chirality. *Top. Curr. Chem.* **2006**, *265*, 209−252.
4. Gellman, A. J. Chiral Surfaces: Accomplishments and Challenges. *ACS Nano* **2010**, *4*, 5–10.
5. Mallat, T.; Orglmeister, E.; Baiker, A. Asymmetric Catalysis at Chiral Metal Surfaces. *Chem. Rev.* **2007**, *107*, 4863–4890.
6. Lämmerhofer, M.; Gargano, A. Monoliths With Chiral Surface Functionalization for Enantioselective Capillary Electrochromatography. *J. Pharm. Biomed. Anal.* **2010**, *53*, 1091–1123.
7. Hazen, R. M.; Sholl, D. S. Chiral Selection on Inorganic Crystalline Surfaces. *Nat. Mater.* **2003**, *2*, 367.
8. Ernst, K.-H. Amplification of Chirality in Two-Dimensional Molecular Lattices. *Curr. Opin. Colloid Interface Sci.* **2008**, *13*, 54–59.
9. Palmans, A. R. A.; Meijer, E. W. Amplification of Chirality in Dynamic Supramolecular Aggregates. *Angew. Chem., Int. Ed.* **2007**, *46*, 8948–8968.
10. Roth, C.; Passerone, D.; Ernst, K. H. Pasteur's Quasiracemates in 2D: Chiral Conflict Between Structurally Different Enantiomers Induces Single-Handed Enantiomorphism. *Chem. Commun.* **2010**, *46*, 8645–8647.
11. Destoop, I.; Ghijsens, E.; Katayama, K.; Tahara, K.; Mali, K. S.; Tobe, Y.; De Feyter, S. Solvent-Induced Homochirality in Surface-Confined Low-Density Nanoporous Molecular Networks. *J. Am. Chem. Soc.* **2012**, *134*, 19568–19571.
12. Katsonis, N.; Xu, H.; Haak, R. M.; Kudernac, T.; Tomović, Ž.; George, S.; Van Der Auweraer, M.; Schenning, A. P. H. J.; Meijer, E. W.; Feringa, B. L.; De Feyter, S. Emerging Solvent-Induced Homochirality by the Confinement of Achiral Molecules against a Solid Surface. *Angew. Chem., Int. Ed.* **2008**, *47*, 4997–5001.
13. Berg, A. M.; Patrick, D. L. Preparation of Chiral Surfaces from Achiral Molecules by Controlled Symmetry Breaking. *Angew. Chem., Int. Ed.* **2005**, *44*, 1821–1823.
14. Fasel, R.; Parschau, M.; Ernst, K.-H. Amplification of Chirality in 2D Enantiomorphous Lattices. *Nature* **2006**, *439*, 449.
15. Haq, S.; Liu, N.; Humblot, V.; Jansen, A. P. J.; Raval, R. Drastic Symmetry Breaking in Supramolecular Organization of Enantiomerically Unbalanced Monolayers at Surfaces. *Nat. Chem.* **2009**, *1*, 409–414.
16. Green, M. M.; Reidy, M. P.; Johnson, R. J.; Darling, G.; Oleary, D. J.; Willson, G. Macromolecular Stereochemistry - the Out-of-Proportion Influence of Optically-Active Co-Monomers on the Conformational Characteristics of Polyisocyanates - the Sergeants and Soldiers Experiment. *J. Am. Chem. Soc.* **1989**, *111*, 6452–6454.
17. Parschau, M.; Romer, S.; Ernst, K.-H. Induction of Homochirality in Achiral Enantiomorphous Monolayers. *J. Am. Chem. Soc.* **2004**, *126*, 15398–15399.
18. Liu, N.; Haq, S.; Darling, G. R.; Raval, R. Direct Visualization of Enantiospecific Substitution of Chiral Guest Molecules into Heterochiral Molecular Assemblies at Surfaces. *Angew. Chem., Int. Ed.* **2007**, *46*, 7613–7616.
19. Parschau, M.; Kampen, T.; Ernst, K. H. Homochirality in Monolayers of Achiral Meso Tartaric Acid. *Chem. Phys. Lett.* **2005**, *407*, 433–437.
20. Tahara, K.; Yamaga, H.; Ghijsens, E.; Inukai, K.; Adisoejoso, J.; Blunt, M. O.; De Feyter, S.; Tobe, Y. Control and Induction of Surface-Confined Homochiral Porous Molecular Networks. *Nat. Chem.* **2011**, *3*, 714–719.
21. De Cat, I.; Guo, Z.; George, S. J.; Meijer, E. W.; Schenning, A. P. H. J.; De Feyter, S. Induction of Chirality in an Achiral Monolayer at the Liquid/Solid Interface by a Supramolecular Chiral Auxiliary. *J. Am. Chem. Soc.* **2012**, *134*, 3171–3177.
22. Chen, T.; Yang, W. H.; Wang, D.; Wan, L. J. Globally Homochiral Assembly of Two-Dimensional Molecular NetworksTriggered by Co-Absorbers. *Nat. Commun.* **2013**, *4*, No. 1389.
23. Seibel, J.; Allemann, O.; Siegel, J. S.; Ernst, K.-H. Chiral Conflict among Different Helicenes Suppresses Formation of One Enantiomorph in 2D Crystallization. *J. Am. Chem. Soc.* **2013**, *135*, 7434–7437.
24. Weigelt, S.; Busse, C.; Petersen, L.; Rauls, E.; Hammer, B.; Gothelf, K. V.; Besenbacher, F.; Linderoth, T. R. Chiral Switching

by Spontaneous Conformational Change in Adsorbed Organic Molecules. *Nat. Mater.* **2006**, *5*, 112–117.
25. Knudsen, M. M.; Kalashnyk, N.; Masini, F.; Cramer, J. R.; Lægsgaard, E.; Besenbacher, F.; Linderoth, T. R.; Gothelf, K. V. Controlling Chiral Organization of Molecular Rods on Au(111) by Molecular Design. *J. Am. Chem. Soc.* **2011**, *133*, 4896–4905.
26. Masini, F.; Kalashnyk, N.; Knudsen, M. M.; Cramer, J. R.; Lægsgaard, E.; Besenbacher, F.; Gothelf, K. V.; Linderoth, T. R. Chiral Induction by Seeding Surface Assemblies of Chiral Switches. *J. Am. Chem. Soc.* **2011**, *133*, 13910–13913.
27. Bombis, C.; Weigelt, S.; Knudsen, M. M.; Nørgaard, M.; Busse, C.; Lgsgaard, E.; Besenbacher, F.; Gothelf, K. V.; Linderoth, T. R. Steering Organizational and Conformational Surface Chirality by Controlling Molecular Chemical Functionality. *ACS Nano* **2010**, *4*, 297–311.
28. Busse, C.; Weigelt, S.; Petersen, L.; Lægsgaard, E.; Besenbacher, F.; Linderoth, T. R.; Thomsen, A. H.; Nielsen, M.; Gothelf, K. V. Chiral Ordering and Conformational Dynamics for a Class of Oligo-phenylene-ethynylenes on Au(111). *J. Phys. Chem. B* **2007**, *111*, 5850–5860.